Research Article Vol. 12, No. 2 / 1 Feb 2022 / Optical Materials Express 811
Optical Materials EXPRESS

Broadband polarization-insensitive and oblique-incidence terahertz metamaterial absorber with multi-layered graphene

XIAOJUN HUANG,[1,5] MIAO CAO,[1] DANQI WANG,[2] XUEWEN LI,[3] JINGDAO FAN,[3] AND XIAOYAN LI[4,6]

[1]College of Communication and Information Engineering, Xi'an University of Science and Technology, Xi'an, Shaanxi, 710054, China
[2]College of Physics and Electrical Engineering, Xinjiang Normal University, Urumqi, Xinjiang, 830054, China
[3]College of Safety Science and Engineering, Xi'an University of Science and Technology, Xi'an, Shaanxi, 710054, China
[4]College of Physical Science and Technology, Northwestern Polytechnical University, Xi'an, Shaanxi, 710129, China
[5]hxj@xust.edu.cn
[6]lixiaoyan0521@mail.nwpu.edu.cn

Abstract: Metamaterial absorbers have been widely studied in the past decade and their performances have been incessantly improved in the practical applications. In this paper, we present a broadband terahertz metamaterial absorber based on graphene-polyimide composite structure, and the structure consists of a metal substrate and graphene layers with different sizes separated by two polyimide dielectric layers. The simulation results show that the absorptance of the absorber is greater than 90% in 0.86–3.54 THz with the fractional bandwidth of 121.8%. The absorptance can be adjusted by changing the chemical potential of graphene. In addition, the absorber is insensitive to polarization and still has robust tolerance for the oblique incidence. The equivalent circuit model based on transmission line is introduced to analyze the physics of the designed absorber and the results are in good agreement with the simulations. We believe that the designed absorber is a potential competitive candidate in terahertz energy harvesting and thermal emission.

© 2022 Optica Publishing Group under the terms of the Optica Open Access Publishing Agreement

1. Introduction

Metamaterials (MMs) are normally defined as a kind of composite material consisted of periodic array of resonant structures with sub-wavelength dimensions, which can manifest some unphysical electromagnetic (EM) performances compared with the natural materials [1]. In recent years, MMs have been extensively applied in various fields of optical black hole [2], super lens [3], polarization controlling [4,5], sensing [6], EM stealth [7,8], perfect absorption and so on [9,10]. Since the metamaterial absorber (MA) was firstly presented by Landy in 2008 [11]. MAs are highly concerned because of the tremendous absorption ability and application prospects [12–16]. Up to now, the focus of MAs is still on the performance of the bandwidth, polarization insensitivity, oblique incidence and integration of geometry limits [17–22].

Terahertz technology has been applied in biomedicine [23,24], safety inspection [25] etc. Particularly, many recent reports have placed high hopes on the application of terahertz waves in 6G communications [26,27]. Recently, terahertz MAs are proposed to be possibly applied in ultra-high data rate short-path wireless communication in the field of communication [28]. They also have wide application prospects in energy harvester [29], thermal emission [30], sensor [31] and micro-bolometer [32]. Zhou Qihui et al. presented a tunable broadband terahertz MM absorber based on graphene with transmission band, and its absorption can be tuned from 0.4 to

#451450 https://doi.org/10.1364/OME.451450
Journal © 2022 Received 15 Dec 2021; revised 20 Jan 2022; accepted 23 Jan 2022; published 31 Jan 2022

Optical Materials EXPRESS

0.9 in 0.5–1 THz [33]. Rishi Mishra et al. investigated a terahertz absorber loaded graphene fractal frequency selective surface, which obtained a −10dB reflection coefficient bandwidth of 2.66 THz [34]. Liu Zhongmin et al. proposed a broadband terahertz absorber with singular graphene patches array and metal-backed dielectric substrate, of which the work absorption bandwidth (absorption > 90%) is 0.47 - 1.47 THz with a relative bandwidth of 100% [35]. Yan Dexian et al. also achieved a broadband graphene-based tunable terahertz MA with the absorptance larger than 90% in 0.65–1.3 THz [36]. Zhou Runhua et al. designed a tunable broadband terahertz absorber which is composed of graphene, silicon dioxide and vanadium dioxide. The absorptivity of the absorber can be as high as 90% in a wide range of 0.65 THz [37]. For the manufacturing of terahertz devices, since the size of the unit is much smaller than the wavelength of the incident electromagnetic wave, the fabrication of terahertz devices usually requires complicated and numerous steps and the use of high-cost equipment, such as equipment with functions of focusing ion beams or lithography [38]. Although these devices can make terahertz devices, they are time-consuming, complicated and costly. Therefore, the fabrication of terahertz devices is still a challenge. Although the above-mentioned literatures all use different methods to achieve broadband absorption in terahertz frequency, the MAs are still suffering from the narrow relative bandwidth and awful oblique incidence, to some extent, which limits the practical applications. It is still highly desirable to design ultra-wideband terahertz absorber with excellent incident performance.

In this work, we present a broadband terahertz MA based on graphene-polyimide composite structure. The absorptance of the MA in 0.86−3.54 THz band is greater than 90% with the fractal bandwidth of 121.8%. The designed MA is insensitive to polarization and still shows excellent oblique incidence robustness. Compared the previous works, our MA has the wider bandwidth and incident angle (TM). The simulation results show that the absorptance can be adjusted with changing the chemical potential of graphene layers. Our designed absorber has the applications in terahertz energy harvesting and thermal emission.

2. Design and simulation

Figure 1 shows a structural unit cell of the designed MA. The MA is composed of three graphene-polyimide composite layers, shown in Fig. 1(a). The first layer a nine-small square pillars graphene-polyimide composite structure. The second layer is a graphene mesh-polyimide layer, and the third layer is a common graphene-polyimide layer. The metal backboard of gold ($\sigma = 4.561\times10^7$ S/m) with thickness of 1μm is covered on the bottom for preventing the transmission. The geometries in Fig. 1(b) are optimized as following: $p = 118$ μm, $w_1 = 26$ μm, $w_2 = 37$ μm, $h_1 = 29.8$ μm, $h_2 = 15.4$ μm and $h_3 = 24$ μm. The thickness of the graphene on each layer is 0.07 μm and the polyimide layer is modeled with $\varepsilon_r = 3.5$ and the $\tan\delta = 0.0027$.

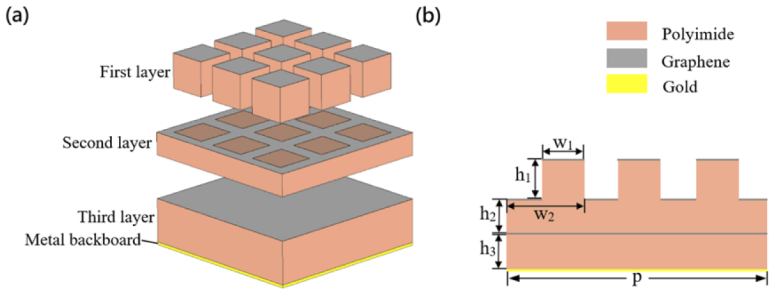

Fig. 1. Unit cell schematic of the broadband graphene terahertz absorber. (a)The three-dimensional diagram of the MA. (b)The cross section of the MA.

Optical Materials EXPRESS

In the simulation, we carry out the simulation by using by the software CST Microwave Studio. The reflectance and absorptance of the MA are simulated and calculated by using frequency domain analyzer of tetrahedral grid. In the x and y axes, boundary conditions are set as unit cell. An open boundary condition (open add space) is applied in the Z-max direction, and the Z-min direction is set to be grounded (Et = 0).

3. Results and discussion

The absorptance is calculated as $A = 1 - R - T = 1 - |S_{11}|^2 - |S_{21}|^2$, where R and T are the reflection and transmission, and S_{11} and S_{12} are the corresponding reflectance and transmittance. The transmittance S_{12} is equal to zero due to that the thickness of gold plate is far thicker than skin depth. Hence, absorptance of the MA is calculated by $A = 1 - R = 1 - |S_{11}|^2$. To better illustrate the role of each graphene layer, we simulate the absorption performance of the model when only each graphene layer is left, as shown in Fig. 2(a). From the figure, the structure cannot absorb electromagnetic waves without graphene, but once graphene is added, it can absorb electromagnetic waves. When only the first, second and third graphene layers are added, their absorption bands (absorptance greater than 0.9) are 1.6–2.2THz, 0.7–1.1THz and 2.3–3.1THz, 1.1–2.2THz, respectively. Figure 2(b) shows that this broadband absorption is not the simple combination of graphene layers, but the broadband absorption obtained through the interaction of three graphene layers.

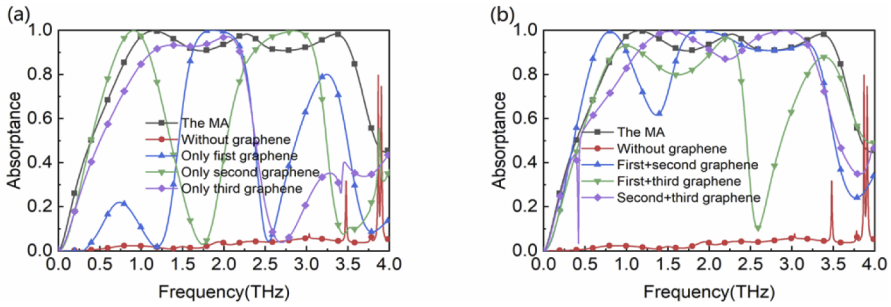

Fig. 2. Absorptance of (a)each graphene layer (b) every two graphene layers.

Figure 3(a) shows the reflectance and absorptance of the MA. We can see that the reflectance is smaller than 0.3 in 0.86–3.54 THz, and the absorptance is greater than 0.9 in this frequency regime. It is known that the perfect absorption will be realized when the equivalent impedance of absorber is matching the impedance of the free space. Herein, we illustrate the equivalent impedance of the MA in Fig. 3(b) to manifest the absorptive performance. It is clearly seen that the real part and imaginary part of the equivalent impedance are nearly 1 and 0, respectively, at the resonant peaks of 1.15 THz, 2.27 THz and 3.35 THz. In addition, the real part and imaginary part of the equivalent impedance are around 1 and 0 in the working frequency scope of 0.86–3.54 THz, respectively. This means that the perfect absorption is achieved in 0.86–3.54 THz because the equivalent impendence of MA is matching the impendence of the free space.

We also discuss the absorptance versus the incidence and polarization. From Fig. 4(a), we can see that the absorptance is greater than 0.8 when the oblique incident angle θ expands to 45° under TE polarization, and the absorptance is still larger than 0.7 when the angle of incidence reaches to 60°. This means that the designed MA has robust tolerance of the oblique incidence. For the TM polarization, shown in Fig. 4(b), the tolerance of the absorptance is extremely better than the TE polarization, and the absorptance is larger than 0.9 when the incident angle reaches to 60°. Apparently, there are some differences between TE and TM polarizations existed under oblique incidence from Fig. 4(a) and 4(b). This is because the dominant resonance of the MA

Optical Materials EXPRESS

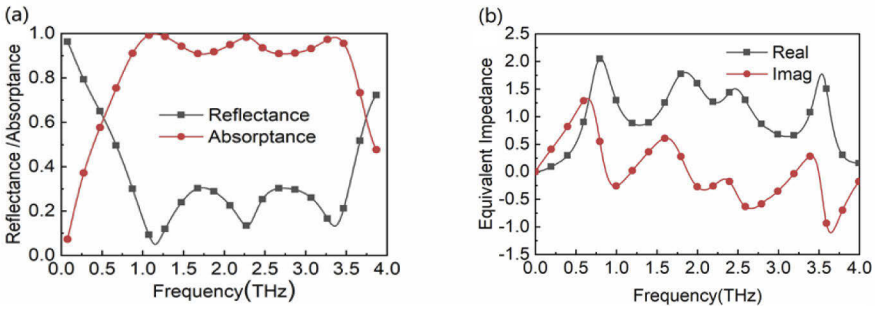

Fig. 3. (a) Reflectance and absorptance (b) Real and imaginary parts of equivalent impedance of the absorber.

is excited by the magnetic field, in other word, the MA is a magnetic resonant absorber. Thus, the absorber has a very stable absorptance (A \gt 0.9 when θ=60°) under TM polarization because of the magnetic field component for exciting the resonance is unchanged. However, the component of magnetic field is gradually decreasing when the oblique incident angle increases in TE polarization, which will lead to the absorptance gradually decreases [39]. Figure 4(c) illustrates the absorptance with different polarizations, we can see that the absorptance is constant with any polarizations due to the C4 design of the MA.

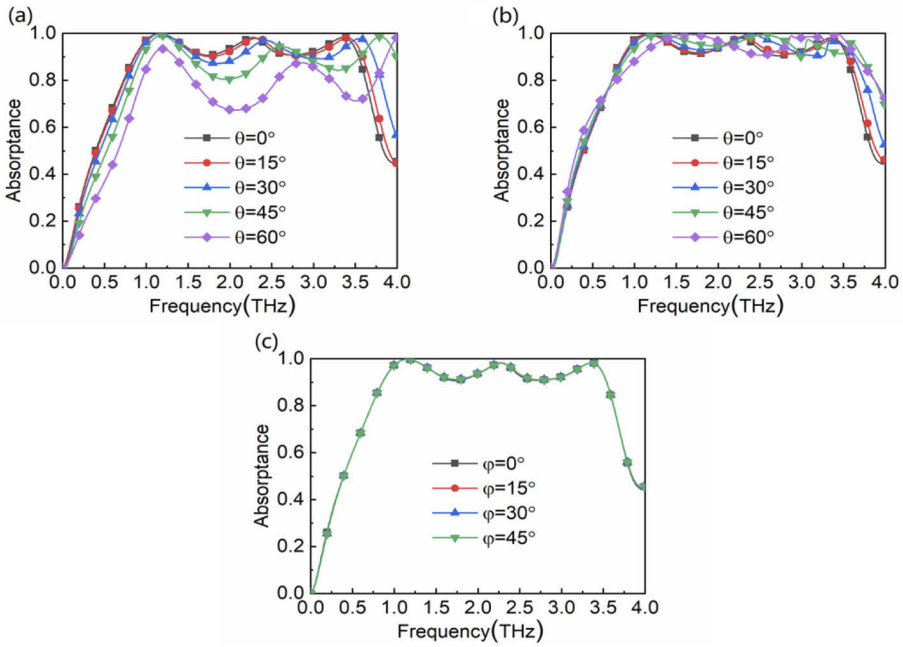

Fig. 4. Absorptance (a)oblique incidence under TE polarization, (b)oblique incidence under TM polarization, (c)under different polarization angles.

We perform the change of the absorptance with adjusting the thickness and periodical size of the MA. Figures 5(a-c) show the influence of the thickness of each layer on the absorptance. We simulate the absorptance with different thickness for each layer with the step of 2 μm while fixing other parameters shown. From Fig. 5(a), we can see that the thickness of the third layer (h_1) mainly influences the absorptance and bandwidth of the MA. With the increase of thickness

Optical Materials EXPRESS

of h_1, for all resonance points, there is a red shift in the working frequency band. But the overall absorptance is improved, especially between the first resonance point and the second resonance point. When the thickness increases from 19 μm to 25 μm, the absorptance between the second resonance point and the third resonance point gradually increases, but when it is above 25 μm the absorptance decreases. Figure 5(b) displays the influence of the thickness of the second layer (h_2) on the absorptance of the MA. It is found that there is a very small red shift at 0–2.25 THz and an obvious red shift at 2.25–4 THz with the increase of the thickness of h_2. The thickness of h_2 almost effects on the absorptance below 2.25 THz, but the bandwidth becomes narrower and the absorptance increases gradually with the increase of thickness above 2.25 THz. Compared with Figs. 5(a-b), the third layer has the similar effect on the absorptance and bandwidth shown in Fig. 5(c). As the thickness increases from 25 μm to 33 μm, the absorptance remains above 0.85 with the gentle vibration in 1.3–3.5 THz. The absorptance is almost not affected by the thickness of h_3 when the frequency is lower than 1.3THz. In addition, there is a slight influence on the bandwidth, and the thickness of h_3 corresponding to the minimum and maximum bandwidth is 25 μm and 27 μm, respectively. Herein, it should be clear that the effect of the first layer is the opposite of the effect of the third layer, meaning that the absorptance is relatively lowest when the thickness of h_1 is minimum, whereas the absorptance is relatively highest when the thickness of h_3 is minimum. Figure 5(d) depicts the influence of the absorptance with the periodical size of the MA from 110 μm to 130 μm with the step of 4 μm. The simulation result shows that the bandwidth of the MA is unchanged but the absorptance is obviously improved with the increase of the periodical size. The absorptance is above 0.9 in 0.86–3.54 THz, and the absorptance reaches to 0.98 at three resonant frequencies of 1.15 THz, 2.27 THz and 3.35 THz, respectively.

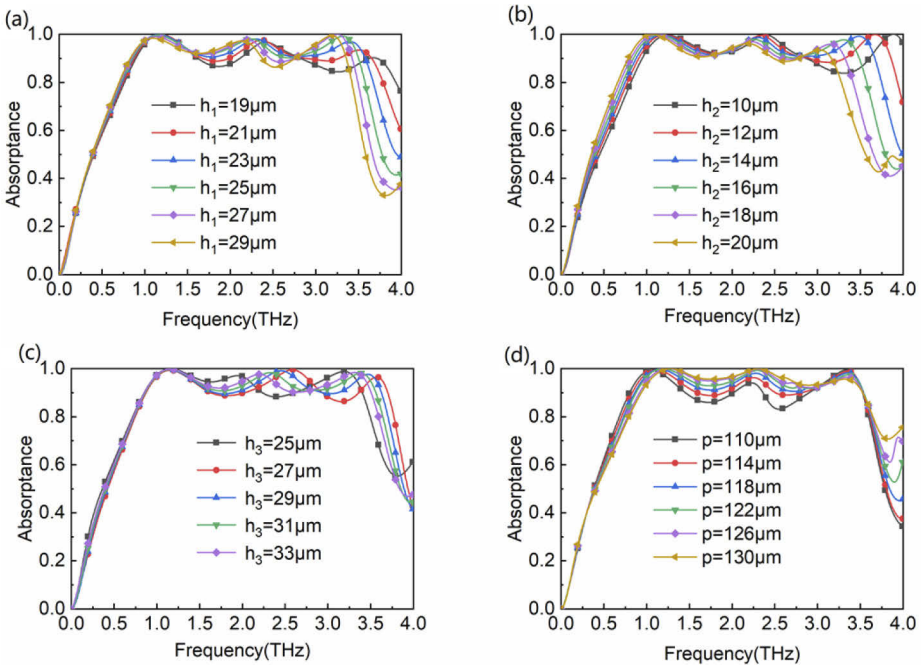

Fig. 5. Absorptance with different geometric parameters. (a) thickness of first layer, (b) thickness of second layer, (c) thickness of third layer, (d) periodic geometry.

In what follows, we explore the influence of graphene layer on the absorptance of the MA. We illustrate the absorptance with different thicknesses of graphene layer while fixing other parameters in Fig. 6(a). We simulate the graphene layer thickness from 0.01 μm and 0.09

Optical Materials EXPRESS

μm with the step of 0.02 μm. It is shown that there is no effect on the absorptance with the thickness of graphene layer. Additionally, we also investigate the influence of chemical potential of graphene layer on the absorptance shown in Fig. 6(b). The absorptance of the absorber changes between 0.15 and 1. Our research range is from 0.0 eV to 1.0 eV, and the absorptance of absorber at different chemical potential is simulated and calculated at intervals of 0.1 eV in Fig. 6(b). Combined with Fig. 6(c) and Fig. 6(d), for the designed absorber, the best absorption performance can be achieved when the chemical potential is 0.9 eV. From Fig. 6(c), it illustrates that chemical potential has a regular influence on resonance frequency. With the improvement of the chemical potential of all graphene layers, the resonance frequencies of three resonance points show a similar linear increase, which shows that the increase of chemical potential has little effect on the absorption bandwidth of the absorber. Figure 6(d) reveals that the chemical potential will affect the absorption performance at each resonance point. Therefore, the designed graphene-loaded MA can be used as a dynamically tunable wave-absorbing device, which indicates that graphene materials have a broader application prospect in the field of tunable devices.

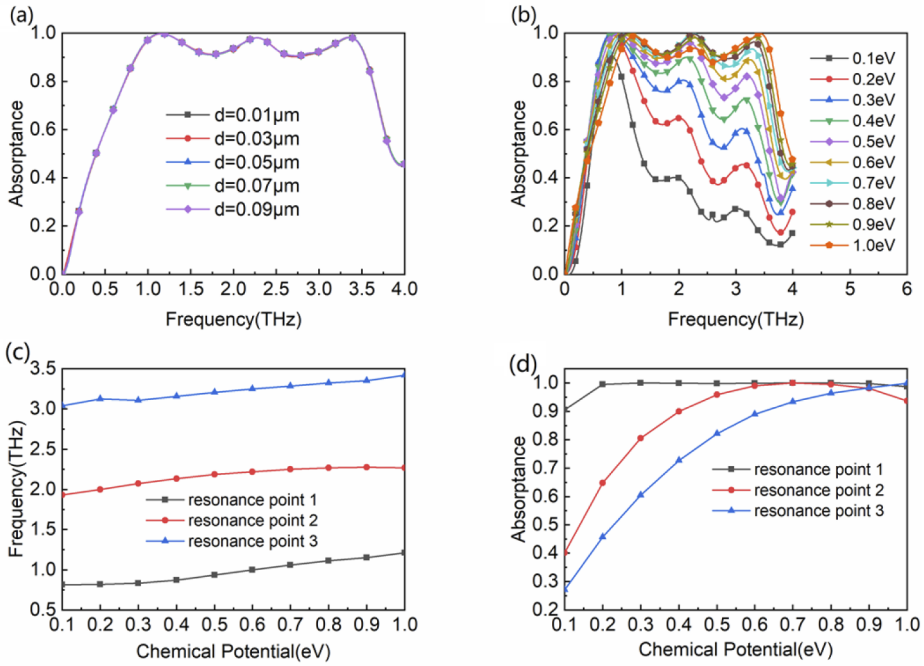

Fig. 6. Absorptance(a)different thickness of graphene layer, (b) different graphene chemical potential; Relations between (c)resonant frequency and chemical potential, (d) absorptance of resonant point and chemical potential.

In order to further explore and demonstrate the absorption mechanism of the MA, we illustrate the distributions of electric field energy and magnetic field energy at three resonance points of 1.15 THz, 2.27 THz and 3.35 THz, respectively. Figure 7 shows the electric field energy distributions of each graphene layers at three resonance frequencies. At the resonance frequency of 1.15 THz, the electric field energy is mostly distributed in graphene of the first layer (graphene patches) and the horizontal stripes of graphene of the second layer (graphene mesh). At 2.27 THz, the electric field energy is mostly distributed in the vertical stripes of graphene mesh, and a small part is distributed in graphene of the first graphene layer and the third graphene layer. At 3.35 THz, it has a similar distribution to that at 2.27 THz.

Optical Materials EXPRESS

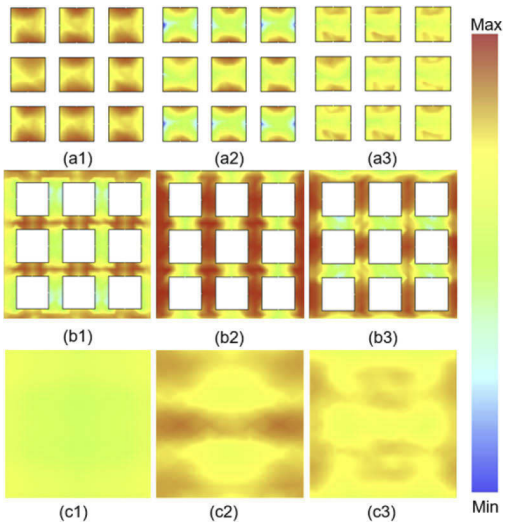

Fig. 7. The electric field energy distribution at 1.15 THz, 2.27 THz and 3.35 THz, respectively. (a1-a3) first layer, (b1-b3) second layer, (c1-c3) third layer.

Figure 8 show the magnetic field energy distributions of graphene layers at three resonance frequencies of 1.15 THz, 2.27 THz and 3.35 THz, respectively. At 1.15 THz, the magnetic field energy distribution is strongest on a certain patch of the graphene patches and the vertical stripes of the graphene mesh. At 2.27 THz, one patch on the first graphene layer has the strongest magnetic field energy, while other patches have strong magnetic field energy. And the edge of the second graphene layer is also distributed with strong magnetic field energy. Compared with the other two resonance points, the magnetic field distribution at 3.35 THz is quite different. There is strong magnetic field energy in the third graphene layer. In a word, the multi-layers of graphene stimulate the several resonances in the working frequency band of the MA which can absorb the EM wave.

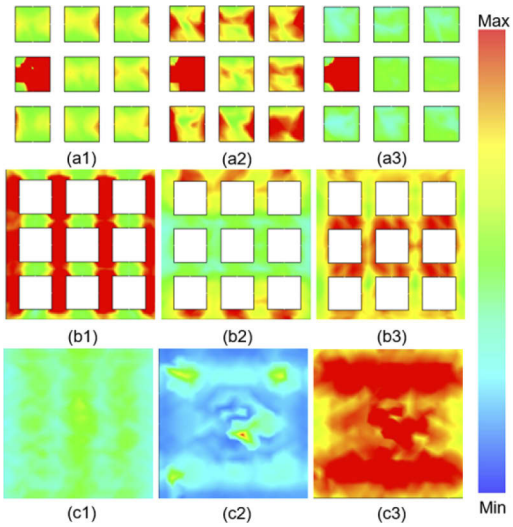

Fig. 8. The magnetic field energy distribution at 1.15 THz, 2.27 THz and 3.35 THz, respectively. (a1-a3) first layer, (b1-b3) second layer, (c1-c3) third layer.

Optical Materials EXPRESS

In order to better prove the excellent performance of the proposed MA, it is necessary to make comparison for the performance of this MA with published graphene-based terahertz MA (see Table I). The relative bandwidth (RB) is defined as $RB = 2 \times (f_H - f_L)/(f_H + f_L)$. Oblique incidence robustness refers to the maximum incident angle that can be achieved when the absorptance of the absorber is kept above 0.8. Compared with other graphene-based terahertz absorbers, the designed absorber in this paper has the widest RB and excellent oblique incidence robustness.

Ref.	RB (%)	BW(THz)	Oblique Incidence Robustness (Absorptance > 0.8)
[33]	66.7	0.5–1	0°–45°(TE,TM)
[34]	110.4	1.08–3.74	0°–45°(TE,TM)
[35]	103.1	0.47–1.47	Not mentioned
[36]	66.7	0.65–1.53	0°–15°(TE,TM)
[37]	49.8	0.98–1.63	0°–50°(TE,TM)
[39]	84.5	1.34–3.4	0°–45°(TE),0°–60°(TM)
[40]	90.3	1.7–4.5	0°–40°(TE),0°–60°(TM)
[41]	93.3	0.8–2.2	Not mentioned
This work	121.8	0.86–3.54	0°–45°(TE),0°–65°(TM)

4. Equivalent circuit model

In this section, we introduce the equivalent circuit model which is based on transmission line (TL) theory to illustrate the absorptance of the designed MA. The surface conductivity of graphene can be divided into inter-band and intra-band contributions, and the total conductivity of graphene is equal to the sum of them. The intra-band surface conductivity is calculated as [42]

$$\sigma_{intra} = -j\frac{e^2 k_B T}{\pi\hbar^2\omega}\left[\frac{\mu_c}{k_B T} + 2\ln(e^{-\mu_c/k_B T} + 1)\right] \tag{1}$$

The inter-band surface conductivity can be approximated for $k_B T \ll |\mu_c|, \omega\hbar$ as

$$\sigma_{inter} \simeq \frac{-je^2}{4\pi\hbar}\ln\left(\frac{2|\mu_c| - \omega\hbar}{2|\mu_c| + \omega\hbar}\right) \tag{2}$$

The intra-band surface conductivity is dominant in the terahertz region, the complex conductivity can be expressed as [43]

$$\sigma_{intra} = \frac{\sigma}{1 + j\omega\tau} \tag{3}$$

where ω is angular frequency and

$$\sigma = \frac{e^2 k_B T\tau}{\pi\hbar^2}\left(\frac{\mu_c}{k_B T} + 2\ln(e^{-\mu_c/k_B T} + 1)\right) \tag{4}$$

In Eq. (4), e, k_B, T, τ, $\hbar$ and μ_c are elementary charge, Boltzmann's constant, temperature, electro-phonon relaxation time, reduced Planck's constant and chemical potential, respectively. Herein, T is set to 300 K, and $\tau = 0.1$ ps.

Optical Materials EXPRESS

The complex impedance of the graphene patches array and the graphene mesh are evaluated as [43,44]

$$Z_{g1} = \frac{D}{(D-g)\sigma} + j\left[\frac{\omega\tau D}{(D-g)\sigma} - \frac{1}{\omega C_{eff}}\right] \tag{5}$$

$$Z_{g2} = \frac{D}{g\sigma} + j\omega\left(\frac{\tau D}{g\sigma} + L_{eff}\right) \tag{6}$$

In Eq. (5), D is the period of the graphene patches array, and g is the width of crack between the patches ($D>g$). From Eq. (5), we mimic the graphene patches as a R-L-C series circuit, in which the R and L are determined by surface conductivity of the graphene patches array. From the literature [44], the graphene mesh attached to the surface of the dielectric layer should be equivalent to an R-L series circuit as shown in Eq. (6). However, the graphene mesh in the proposed absorber is embedded in the dielectric layer instead of attached to the surface of the dielectric layer. Therefore, we added a parameter (C_d) related to medium to Eq. (6), and modified Eq. (6) as

$$Z_{g2} = \frac{D}{g\sigma} + j\omega\left(\frac{\tau D}{g\sigma} + L_{eff}\right) + \frac{1}{j\omega C_d} \tag{7}$$

From Eq. (7), we mimic the graphene mesh as a R-L-C series circuit. The C_{eff} and L_{eff} are influenced by the geometry of the graphene patches. The C_{eff} and L_{eff} can be described by Eq. (8) and Eq. (9). Where the ε_r is the relative dielectric constant of the material around graphene patches [43,44].

$$C_{eff} = \frac{1}{\pi}\varepsilon_0(\varepsilon_r + 1)D\ln\left[\csc\left(\frac{\pi g}{2D}\right)\right] \tag{8}$$

$$L_{eff} = \frac{D\mu_0}{2\pi}\ln\left[\csc\left(\frac{\pi g}{2D}\right)\right] \tag{9}$$

The complex impedance of the dielectric substrate is calculated as [45]

$$Z_d = jZ_c\tan(k_{zp}l) \tag{10}$$

In Eq. (7), $Z_c = \omega\mu_r/k_{zp}$ is the characteristic impedance of the dielectric substrate, in which the $k_{zp} = \sqrt{k_p^2 - k_0^2\sin^2\theta}$ represents the propagation constant along z axis. l is the thickness of the dielectric substrate. k_0 and $k_p = \omega\sqrt{\mu_r\varepsilon_r}$ are the wave number of the incident wave vector in free space and the dielectric substrate, respectively. μ_r and ε_r are relative permeability and relative dielectric coefficient of the dielectric substrate.

In Fig. 9, the equivalent circuit model of the designed absorber is introduced based on the above theory and TL theory. To present equivalent circuit approach for the MA. As shown in

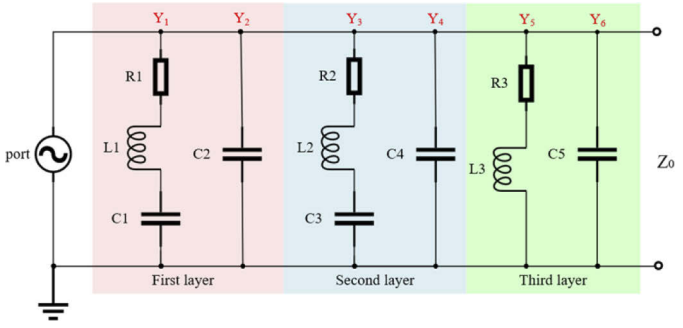

Fig. 9. Equivalent circuit of the absorber.

Optical Materials EXPRESS

Fig. 1(a), we recall generally the structure of the MA, and it consists of three graphene layers separated by polyimide layers. The graphene of first layer is a graphene patches array, and it can be equivalent to a $R-L-C$ series circuit. The graphene of second layer is a graphene mesh, and it also can be equivalent to a $R-L-C$ series circuit. And the third layer is a complete graphene sheet which can be equivalent to a $R-L$ series circuit. Moreover, the dielectric substrates in the first, second and third layers are equivalent to capacitors C2, C4 and C5, respectively.

According to the circuit theory, the admittance analysis of each layer is as follows [45]:

$$Y_1 = \frac{1}{R_1 + j\omega L_1 + 1/j\omega C_1} \tag{11}$$

$$Y_2 = j\omega C_2 \tag{12}$$

$$Y_3 = \frac{1}{R_2 + j\omega L_2 + 1/j\omega C_3} \tag{13}$$

$$Y_4 = j\omega C_4 \tag{14}$$

$$Y_5 = \frac{1}{R_3 + j\omega L_3} \tag{15}$$

$$Y_6 = j\omega C_5 \tag{16}$$

Each layer is connected in parallel with each other, so the equivalent admittance of the MA is expressed as:

$$Y_{in} = Y_1 + Y_2 + Y_3 + Y_4 + Y_5 + Y_6 \tag{17}$$

The equivalent impedance of the MA is expressed as:

$$Z_{in} = \frac{1}{Y_{in}} \tag{18}$$

The coefficient of reflectance can be obtained by

$$\Gamma = \frac{Z_{in} - Z_0}{Z_{in} + Z_0} \tag{19}$$

The expression of absorptance is

$$A = 1 - |\Gamma|^2 \tag{20}$$

The reflection coefficient and absorptance of the circuit are simulated by ADS (Advanced Design System 2016), and compared with that simulated by CST. From Fig. 10, the results obtained by equivalent circuit are very close to those obtained by CST simulation.

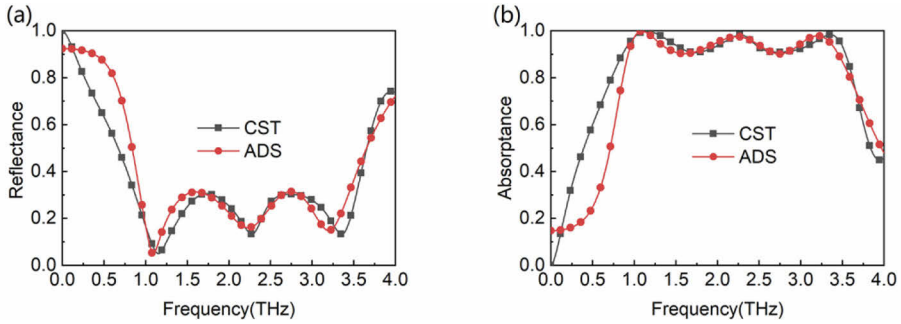

Fig. 10. (a) Reflectance comparison (b) Absorptance comparison.

Optical Materials EXPRESS

5. Conclusion

In summary, we propose a broadband terahertz metamaterial absorber based on graphene-polyimide composite structure layer. The simulation results show that the absorptance of the metamaterial absorber in 0.8–3.3 THz band is greater than 90%, and the absorption bandwidth is about 2.5 THz. The MA is insensitive to polarization and still shows excellent oblique incidence robustness. The loss of the middle dielectric layer of the absorber affects the performance of the absorber, so we analyze the influence of the dielectric layer and the period of the MA. We also discuss the influence of graphene from two angles because the resonance layer is made of graphene. Finally, an equivalent circuit model for the MA is analytically investigated. The design method of the absorber presented may find potential applications in terahertz energy harvesting and thermal emission.

Funding. The Project of Science and Technology of Shaanxi (No.2019JLZ-08, 2021JM-395); The Science and Technology Plan Project of Xi'an Beilin District (GX1926).

Acknowledgments. This work was supported by the Project of Science and Technology of Shaanxi (No.2019JLZ-08, 2021JM-395), the Science and Technology Plan Project of Xi'an Beilin District (GX1926).

Disclosures. The authors declare no conflicts of interest.

Data availability. Data underlying the results presented in this paper are not publicly available at this time but may be obtained from the authors upon reasonable request.

References

1. D. R. Smith, W. J. Padilla, D. C. Vier, S. C. Nemat-Nasser, and S. Schultz, "Composite medium with simultaneously negative permeability and permittivity," Phys. Rev. Lett. **84**(18), 4184–4187 (2000).
2. W. Yang, J. Li, and Y. Huang, "Modeling and analysis of the optical black hole in metamaterials by the finite element time-domain method," Comput. Methods Appl. Mech. Eng. **304**, 501–520 (2016).
3. Y. Li and Q. Zhu, "Broadband birefringent metamaterial lens with bi-functional high-gain radiation and deflection properties," Opt. Express **26**(13), 16265–16276 (2018).
4. L. Peng, X. F. Li, X. Jiang, and S. M. Li, "A novel THz half-wave polarization converter for cross-polarization conversions of both linear and circular polarizations and polarization conversion ratio regulating by graphene," J. Light. Technol. **36**(19), 4250–4258 (2018).
5. J. Bai and Y. Yao, "Highly efficient anisotropic chiral plasmonic metamaterials for polarization conversion and detection," ACS Nano **15**(9), 14263–14274 (2021).
6. A. M. Albishi, M. K. E. Badawe, V. Nayyeri, and O. M. Ramahi, "Enhancing the sensitivity of dielectric sensors with multiple coupled complementary split-ring resonators," IEEE Trans. Microw. Theory Tech. **68**(10), 4340–4347 (2020).
7. D. Winson, B. Choudhury, N. Selvakumar, H. Barshilia, and R. U. Nair, "Design and development of a hybrid broadband radar absorber using metamaterial and graphene," IEEE Trans. Antennas Propag. **67**(8), 5446–5452 (2019).
8. Y. Zhou, J. Chen, R. Chen, W. Chen, Z. Fan, and Y. Ma, "Ultrathin electromagnetic–acoustic amphibious stealth coats," Adv. Opt. Mater. **8**(15), 2000200 (2020).
9. L. Chen, S. W. Qu, B. J. Chen, X. Bai, K. B. Ng, and C. H. Chan, "Terahertz metasurfaces for absorber or reflectarray applications," IEEE Trans. Antennas Propag. **65**(1), 234–241 (2017).
10. S. Xiao, T. Liu, L. Cheng, C. Zhou, X. Jiang, Z. Li, and C. Xu, "Tunable anisotropic absorption in hyperbolic metamaterials based on black phosphorous/dielectric multilayer structures," J. Light. Technol. **37**(13), 3290–3297 (2019).
11. N. I. Landy, S. Sajuyigbe, J. J. Mock, D. R. Smith, and W. J. Padilla, "Perfect metamaterial absorber," Phys. Rev. Lett. **100**(20), 207402 (2008).
12. L. Zhou and Z. Shen, "Hybrid frequency-selective rasorber with low-frequency diffusion and high-frequency absorption," IEEE Trans. Antennas Propag. **69**(3), 1469–1476 (2021).
13. L. Feng, P. Huo, Y. Liang, and T. Xu, "Photonic metamaterial absorbers: morphology engineering and interdisciplinary applications," Adv. Mater. **32**(27), 1903787 (2020).
14. J. Xiao, R. Xiao, R. Zhang, Z. Shen, W. Hu, L. Wang, and Y. Lu, "Tunable terahertz absorber based on transparent and flexible metamaterial," Chinese Opt. Lett. **18**(9), 092403 (2020).
15. S. Barzegar-Parizi, A. Ebrahimi, and K. Ghorbani, "High-Q dual-band graphene absorbers by selective excitation of graphene plasmon polaritons: Circuit model analysis," Opt. Laser Technol. **132**, 106483 (2020).
16. S. Barzegar-Parizi and A. Ebrahimi, "Terahertz high-Q absorber based on holes array perforated into a metallic slab," Electron. **10**(15), 1860 (2021).

Optical Materials EXPRESS

17. A. Ghobadi, H. Hajian, M. Gokbayrak, S. A. Dereshgi, A. Toprak, B. Butun, and E. Ozbay, "Visible light nearly perfect absorber: an optimum unit cell arrangement for near absolute polarization insensitivity," Opt. Express **25**(22), 27624–27634 (2017).
18. N. Hu, F. Wu, L. Bian, H. Liu, and P. Liu, "Dual broadband absorber based on graphene metamaterial in the terahertz range," Opt. Mater. Express **8**(12), 3899–3909 (2018).
19. W. Wang, H. Wang, P. Yu, K. Sun, X. Tong, F. Lin, C. Wu, Y. You, W. Xie, Y. Li, C. Yuan, A. O. Govorov, O. L. Muskens, H. Xu, S. Sun, and Z. Wang, "Broadband thin-film and metamaterial absorbers using refractory vanadium nitride and their thermal stability," Opt. Express **29**(21), 33456–33466 (2021).
20. Z. Song and J. Zhang, "Achieving broadband absorption and polarization conversion with a vanadium dioxide metasurface in the same terahertz frequencies," Opt. Express **28**(8), 12487–12497 (2020).
21. S. Barzegar-Parizi, A. Ebrahimi, and K. Ghorbani, "Dual-broadband and single ultrawideband absorbers from the terahertz to infrared regime," J. Opt. Soc. Am. B **38**(9), 2628 (2021).
22. S. Quader, M. R. Akram, F. Xiao, and W. Zhu, "Graphene based ultra-broadband terahertz metamaterial absorber with dual-band tunability," J. Opt. (United Kingdom **22**(9) (2020).
23. K. Ajito, "Terahertz spectroscopy for pharmaceutical and biomedical applications," IEEE Trans. Terahertz Sci. Technol. **5**(6), 1140–1145 (2015).
24. S. Sung, S. Dabironezare, N. Llombart, S. Selvin, N. Bajwa, S. Chantra, B. Nowroozi, J. Garritano, J. Goell, A. Li, S. X. Deng, E. Brown, W. S. Grundfest, and Z. D. Taylor, "Optical system design for noncontact, normal incidence, THz imaging of in vivo human cornea," IEEE Trans. Terahertz Sci. Technol. **8**(1), 1–12 (2018).
25. S. Shishanov, A. Bystrov, E. G. Hoare, A. Stove, M. Gashinova, M. Cherniakov, T. Y. Tran, and N. Clarke, "Height-finding for automotive THz radars," IEEE Trans. Intell. Transp. Syst. **20**(3), 1170–1180 (2019).
26. Z. Zhang, Y. Xiao, Z. Ma, M. Xiao, Z. Ding, X. Lei, G. K. Karagiannidis, and P. Fan, "6G wireless networks: vision, requirements, architecture, and key technologies," IEEE Veh. Technol. Mag. **14**(3), 28–41 (2019).
27. M. Polese, J. M. Jornet, T. Melodia, and M. Zorzi, "Toward end-to-end, full-stack 6G terahertz networks," IEEE Commun. Mag. **58**(11), 48–54 (2020).
28. M. Amiri, F. Tofigh, N. Shariati, J. Lipman, and M. Abolhasan, "Review on metamaterial perfect absorbers and their applications to IoT," IEEE Internet Things J. **8**(6), 4105–4131 (2021).
29. M. Bağmancı, M. Karaaslan, E. Ünal, O. Akgol, F. Karadağ, and C. Sabah, "Broad-band polarization-independent metamaterial absorber for solar energy harvesting applications," Phys. E Low-Dimensional Syst. Nanostructures **90**, 1–6 (2017).
30. R. na Dao, X. ru Kong, H. feng Zhang, and X. ran Su, "A tunable broadband terahertz metamaterial absorber based on the vanadium dioxide," Optik (Stuttg **180**, 619–625 (2019).
31. M. Nejat and N. Nozhat, "Ultrasensitive THz refractive index sensor based on a controllable perfect MTM absorber," IEEE Sens. J. **19**(22), 10490–10497 (2019).
32. C. Chen, Y. Huang, K. Wu, T. G. Bifano, S. W. Anderson, X. Zhao, and X. Zhang, "Polarization insensitive, metamaterial absorber-enhanced long-wave infrared detector," Opt. Express **28**(20), 28843–28857 (2020).
33. Q. Zhou, S. Zha, P. Liu, C. Liu, L. an Bian, J. Zhang, H. Liu, and L. Ding, "Graphene based controllable broadband terahertz metamaterial absorber with transmission band," Materials **11**(12), 2409 (2018).
34. R. Mishra and R. Panwar, "Investigation of graphene fractal frequency selective surface loaded terahertz absorber," Opt. Quantum Electron. **52**(6), 317 (2020).
35. Z. Liu, L. Guo, and Q. Zhang, "A simple and efficient method for designing broadband terahertz absorber based on singular graphene metasurface," Nanomaterials **9**(10), 1351 (2019).
36. D. Yan and J. Li, "Tuning control of broadband terahertz absorption using designed graphene multilayers," J. Opt. (United Kingdom **21**(7), 075101 (2019).
37. R. Zhou, T. Jiang, Z. Peng, Z. Li, M. Zhang, S. Wang, L. Li, H. Liang, S. Ruan, and H. Su, "Tunable broadband terahertz absorber based on graphene metamaterials and VO_2," Opt. Mater. (Amst **114**, 110915 (2021).
38. C. Chen, M. Chai, M. Jin, and T. He, "Terahertz metamaterial absorbers," Adv Mater. Technol. **4**, 2101171 (2021).
39. L. Ye, X. Chen, G. Cai, J. Zhu, N. Liu, and Q. H. Liu, "Electrically tunable broadband terahertz absorption with hybrid-patterned graphene metasurfaces," Nanomaterials **8**(8), 562 (2018).
40. J. Z. X. Q. Y. Wang, S. Chandrasekaran, S. Ramanathan, T. Basak, R. M. V. G. K. Rao, S. Rao, B. K. Sridhara, Y. Li, L. Cheng, J. Zhou, J. Sun, W. Wang, and Q. Yue, "Graphene-based single-layer elliptical pattern metamaterial absorber for adjustable broadband absorption in terahertz range," Int. J. Adv. Manuf. Technol. **25**(7), 783–795 (2018).
41. M. S. Zanjani, I. Chaharmahali, S. Biabanifard, and S. E. Hosseini, "A reconfigurable multi-band, multi-bias THz absorber," Optik (Stuttg **191**(5), 22–32 (2019).
42. G. W. Hanson, "Dyadic Green's functions and guided surface waves for a surface conductivity model of graphene," J. Appl. Phys. **103**(6), 064302 (2008).
43. X. Huang, X. Zhang, Z. Hu, M. Aqeeli, and A. Alburaikan, "Design of broadband and tunable terahertz absorbers based on graphene metasurface: Equivalent circuit model approach," IET Microwaves Antennas Propag. **9**(4), 307–312 (2015).
44. O. Luukkonen, C. Simovski, G. Granet, G. Goussetis, D. Lioubtchenko, A. V. Räisänen, and S. A. Tretyakov, "Simple and accurate analytical model of planar grids and high-impedance surfaces comprising metal strips or patches," IEEE Trans. Antennas Propag. **56**(6), 1624–1632 (2008).
45. H. Xiong, M. C. Tang, M. Li, D. Li, and Y. N. Jiang, "Equivalent circuit method analysis of graphene-metamaterial (GM) absorber," Plasmonics **13**(3), 857–862 (2018).

202.119.44.45 {ts '2022-02-17 09:06:47'}